THE JOURNAL OF PHYSICAL CHEMISTRY A

Article

The Role of the Amino Protecting Group During Para-Hydrogenation of Protected Dehydroamino acids

Erika Cerutti, Alessandra Viale, Carlo Nervi, Roberto Gobetto, and Silvio Aime

J. Phys. Chem. A, **Just Accepted Manuscript** • DOI: 10.1021/acs.jpca.5b06802 • Publication Date (Web): 28 Oct 2015

ACS Publications

The Journal of Physical Chemistry A is published by the American Chemical Society. 1155 Sixteenth Street N.W., Washington, DC 20036

The Role of the Amino Protecting Group during Parahydrogenation of Protected Dehydroamino Acids

Erika Cerutti,[a] *Alessandra Viale,**[,a] *Carlo Nervi,**[b] *Roberto Gobetto,*[b] *Silvio Aime*[a]

Department of Molecular Biotechnologies and Health Sciences, University of Torino, Via Nizza 52 – 10126 Torino – Italy

KEYWORDS: PHIP; DFT; hydrogenation mechanism; amino acids

ABSTRACT

A series of dehydroamino acids endowed with different protective groups at the amino and carboxylate moieties and with different substituents at the double bond have been reacted with parahydrogen. The observed ParaHydrogen Induced Polarization (PHIP) effects in the ^{1}H NMR spectra are strongly dependent on the amino protecting group. DFT calculations allowed to establish a relationship between the structures of the reaction intermediates (whose energies depend on the amido substitution) and the observed PHIP patterns.

Introduction

Hyperpolarization NMR methodologies continue to be under intense scrutiny. A major driving force is represented by the possibility of overcoming the intrinsic low sensitivity of the NMR technique, as high signal enhancements can be obtained upon the application of hyperpolarization procedures. Several methods are currently being used to generate hyperpolarized molecules, including Optical Pumping and Spin Exchange (SEOP) of noble gases, Dynamic Nuclear Polarization (DNP), ParaHydrogen Induced Polarization (PHIP) and Signal Amplification By Reversible Exchange (SABRE). [1-6] From the technologial point of view, among these modalities PHIP is the less demanding one, as it relies on the hydrogenation of unsaturated substrates by using hydrogen enriched in its singlet spin state (parahydrogen). This reaction yields products where both ^{1}H and heteronuclei NMR resonances can be greatly enhanced.[4,5] A number of studies on hyperpolarized molecules have been reported, for the elucidation of chemical reactions mechanisms (by taking advantage of the detection of intermediates at very low concentrations),[4] for the set-up of novel analytical protocols[7] and in the Magnetic Resonance Imaging field.[5]

In the latter field, the search for hyperpolarized molecules is mainly oriented towards substrates of metabolic interest. Pyruvate[6] and lactate[8] generated by the DNP approach, and succinate[9] generated by PHIP are the most relevant hyperpolarized biomolecules. Of course amino acids are also of great potential interest, and some examples of amino acids hyperpolarized by the DNP method are reported.[10,11]

The most straightforward precursors for the preparation of hyperpolarized amino acids by PHIP are the corresponding dehydroamino acids. The use of proper protecting groups at the

amino and carboxylate functionalities is required in order to attain high hydrogenation yields. Up to now, parahydrogen induced polarization in amino acids has been investigated for elucidating the reaction mechanism,[12] in the case of unsaturated precursors of protected alanine,[12] in a small peptide with antibiotic properties,[15] in some neurotransmitters,[16,17] in bioactive peptides labelled with propargyl-amino acids,[18] in ester derivatives of amino acids in water,[19] and in some amino acids and peptides by the SABRE methodology.[20]

Here, the PHIP effects observed in the parahydrogenation of a number of protected amino acids are reported, establishing a correlation between the observed effects and the reaction pathway. On the ground of these results it is evidenced that the effects of the protective groups should be taken into account in the development of a PHIP-based efficient hyperpolarization protocol for natural amino acids.

Results

^{1}H PHIP experiments

A series of dehydroamino acids (**LNa**, where N=1-11) have been reacted with parahydrogen to afford the corresponding hydrogenated derivatives **LNe** (chart 1). Protecting groups on both the carboxylic and the amino groups have been introduced in order to carry out the parahydrogenation reactions in organic solvents. Removal of the carboxylate protection by hydrolysis in basic conditions affords water-soluble substrates which have also been tested for parahydrogenation in water solution.

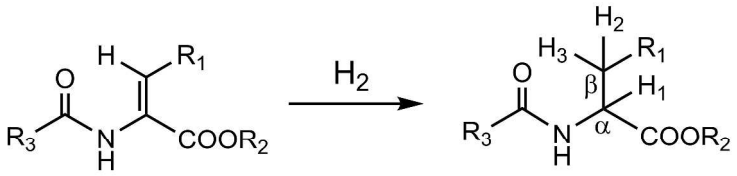

L1a: R_1 = Ph, R_2 = CH_3, R_3 = Ph — **L1e**
L2a: R_1 = Ph, R_2 = CH_3, R_3 = CH_3 — **L2e**
L3a: R_1 = Ph, R_2 = CH_3, R_3 = H — **L3e**
L4a: R_1 = Ph, R_2 = CH_3, R_3 = t-BuO — **L4e**
L5a: R_1 = Ph, R_2 = H, R_3 = Ph — **L5e**
L6a: R_1 = Ph, R_2 = H, R_3 = CH_3 — **L6e**
L7a: R_1 = Ph, R_2 = H, R_3 = H — **L7e**
L8a: R_1 = CH_3, R_2 = CH_3, R_3 = Ph — **L8e**
L9a: R_1 = CH_3, R_2 = CH_3, R_3 = H — **L9e**
L10a: R_1 = H, R_2 = CH_3, R_3 = H — **L10e**
L11a: R_1 = H, R_2 = CH_3, R_3 = CF_3 — **L11e**

Chart 1. Dehydroamino acids for parahydrogenation.

Parahydrogenation reactions have been carried out using ALTADENA conditions[21] by using either [1,4-bis(diphenylphosphino)butane](1,5-cyclooctadiene)rhodium(I) tetrafluoroborate or [(1,4-bis[(phenyl-3-propanesulfonate)phosphine]butane](norbornadiene)rhodium(I) tetrafluoroborate as catalysts in deuterated organic solvent (acetone, methanol, chloroform) and water (D_2O), respectively. Single scan ^1H spectra have been acquired in order to observe the PHIP patterns.

10 mM solutions of all the derivatives **L1a-L11a** have been hydrogenated to the corresponding saturated products **L1e-L11e** in 100% yield after 10 seconds reaction in all the solvents but chloroform, where the reaction has been found to continue also during spectra acquisition, thus affording a PASADENA[22] pattern in the ^1H NMR spectra, with an overall hydrogenation yield of about 50%.

In acetone, methanol and water, the ^1H PHIP pattern is strongly dependent on the nature of the amino protective group, with no relevant solvent effect. When R_3 is a methyl (**L2**) or a proton

(**L3**, **L9**), net absorption / emission signals typical of the ALTADENA experiments are observed for the three protons of the product molecules (Figure 1, spectra b, c, f), while when R_3 is a phenyl (**L1**, **L8**) or a t-butanoyl (**L4**) moiety, each of the H_1, H_2 and H_3 proton signals appears as an antiphase peak, (figure 1, spectra a, d and e). Similar results are obtained for R_1 = phenyl and R_1 = methyl, indicating that the substitution at the amino acid chain does not strongly affect the PHIP pattern of H_1,H_2 and H_3 protons. Nevertheless, on going for example from **L3** to **L9** to **L10** (R_1 = Ph, CH_3 and H respectively), signal enhancements become progressively lower, down to zero in **L10e** (see table 1). As a consequence of this general trend, polarization which is transferred to R_1, via isotropic mixing and possibly dipolar interaction, is finally detected only in **L3** but not in **L9**. Being the T_1 values for **L3**, **L9** and **L10** quite similar (10.0 s, 12.5 s and 10.5 s respectively for H_1, 2.7/2.6 s, 2.3/2.5 s and 3.4 s respectively for H_2/H_3, see table S1 in supporting information), the observed reduction in signal enhancement can not be accounted for by the relaxation properties of the compounds, but rather on the basis of the reaction rates, as it will be outlined below: slowly-reacting compounds result to be less polarized due to polarization loss during the reaction pathway.

In the case of R_3 = H (**L3**, **L7**, **L9**) the formyl proton results to be polarized as well (spectra c and f in figure 1, table 1, figure S3 in supporting information). Polarization can be transferred to the formyl proton through the network of spin-spin couplings and possibly by dipolar interaction. When R_2 = H (**L7**), the signal enhancement is observed predominantly at the formyl proton (see figure S3 in supporting information). In this case, as in **L5** and **L6**, the presence of a COOH group influences the relaxation characteristics of the systems, causing a shortening of the T_1 values for H_1, H_2 and H_3 which prevents polarization to be preserved on these positions (see figures S1 and S2 supporting information).

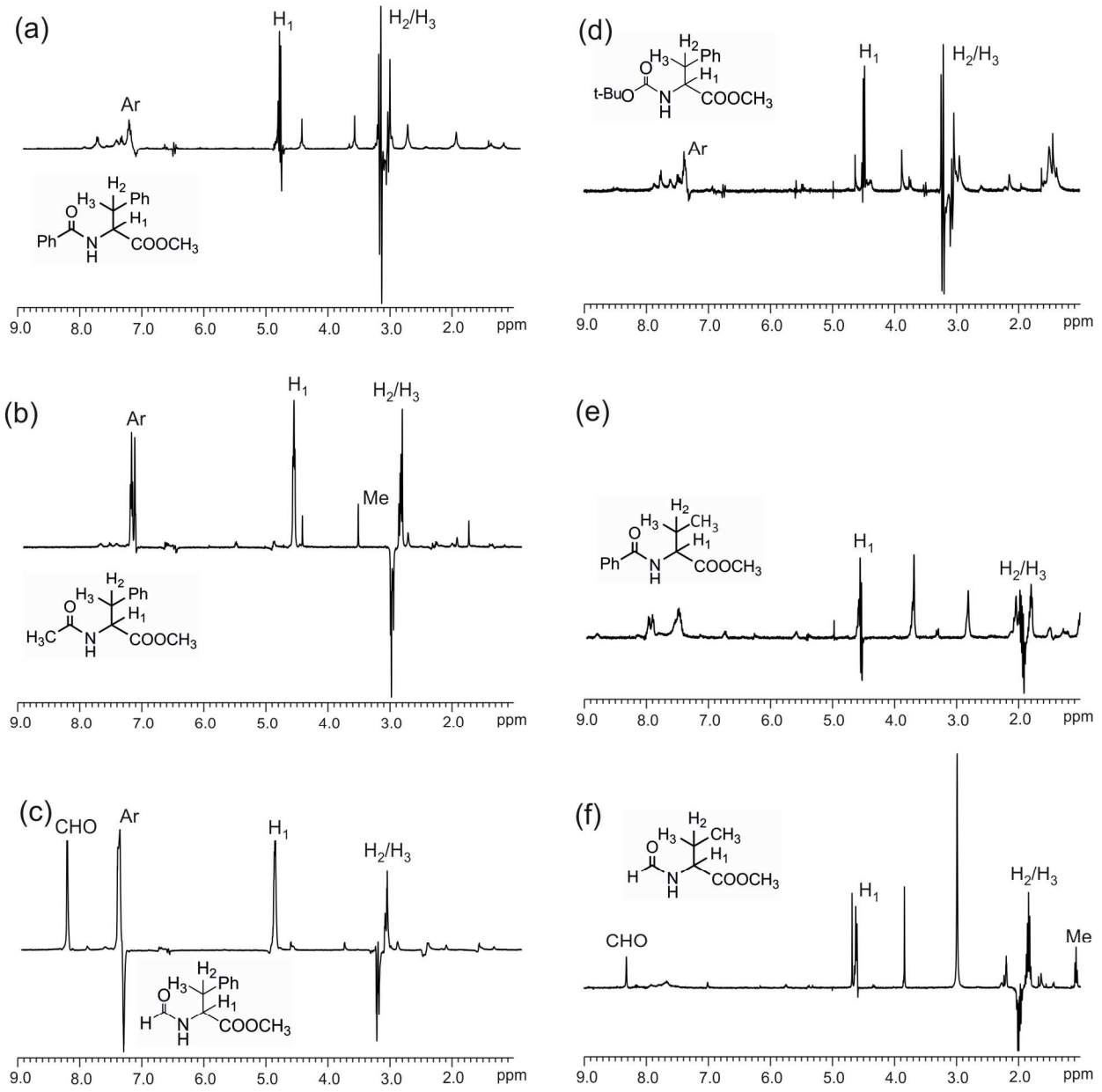

Figure 1. Single scan ^{1}H NMR spectra of hyperpolarized (a) **L1e**, (b) **L2e**, (c) **L3e**, (d) **L4e**, (e) **L8e** and (f) **L9e** (10 mM solutions, RT, 9.4 T; acetone-d_6). No additional information is present in the omitted parts of the spectra.

Compound	Ar	H_1	H_2/H_3	formyl
L1e	1.4	5.2	7.0/6.3	N/A
L2e	4.8	24.5	18.1/18.9	N/A
L3e	10.0	20.1	13.0/13.2	13.4
L4e	2.1	9.3	10.2/11.9	N/A
L5e	1	1	1	N/A
L6e	~1	1	1	N/A
L7e	2.3	~1	1	17.3
L8e	1	4.9	2.5/2.7	N/A
L9e	N/A	6.5	5.4/6.7	2.3
L10e	N/A	1	1	1
L11e	N/A	20.9	23.4/21.2	N/A

Table 1. Proton signal enhancements for compounds **Lne**, calculated as the ratios between the integrals in the polarized spectra and in spectra of relaxed products (a value of 1 indicates that the proton is not polarized).

When R_1 = H (**L10**), no enhanced signals are observed under these experimental conditions (see figure S4 in supporting information). This is not the case for R_1 = H, R_3 = CF_3 (compound **L11**), where ^{1}H net PHIP signals are observed for H_1 and the just formed methyl group (figure S5 in supporting information). Also in this case, relaxation measurements show that this behaviour can not be accounted for by the T_1 values of H_1, H_2, H_3 in **L10e** and **L11e**, as they are quite similar (10.5 s and 12.4 s respectively for H_1, 3.4 s and 3.0 s respectively for the just formed methyl group). We can surmise that the strongly electron-attracting CF_3 group on the amidic CO influences the reaction mechanism and/or the lifetime of the involved intermediates reducing the overall reaction time and thus limiting the polarization loss due to relaxation. Evidence will be given below.

DFT studies of the reaction mechanism

To get more insight into the determinants of the observed effects, we have computationally assessed the effect of the protective group R_3 on the reaction mechanism. The evaluation of the energies of intermediates and transition states along the reaction pathway allows to extract information about the role of R_3 in determining the observed PHIP patterns. As no effect of R_1 on the pattern of H_1, H_2 and H_3 protons has been experimentally evidenced, the calculations have been initially performed on a reference substrate, where $R_1 = R_2 = R_3 = CH_3$ (**L0a**), and then extended to the set of deyhydroamino acids subjected to the parahydrogenation reactions.

The general hydrogenation mechanism (scheme 1), as found from the calculation results, involves the formation of the η-H_2 complexes **a** (figure 2), which are then transformed into the dihydride species **b**. Dihydride intermediates in the parahydrogenation of unsaturated amino acids have been previously detected by Giernoth et al.[12] In the present case, two different dihydride intermediates may be formed at this stage: in the first one ($\mathbf{b_C}$) the equatorial hydride is on the same side of the β sp^2 carbon atom, while in the second one ($\mathbf{b_N}$) the equatorial hydride is on the side of the α sp^2 carbon atom. The pathways leading to $\mathbf{b_C}$ and $\mathbf{b_N}$ will be called "C route" and "N route" respectively. In both cases, the **b** intermediates have very low lifetimes, as the transfer of the first hydrogen atom to the C=C double bond giving the monohydride intermediates **c** (either $\mathbf{c_C}$ or $\mathbf{c_N}$), is very fast for all the substrates. The third reaction step is a rotation of the monohydrogenated products around the residual Rh-C bond, giving the rearranged monohydrides $\mathbf{d_C}$ and $\mathbf{d_N}$ respectively. Then, transfer of the second hydrogen atom from the metal to the substrate occurs, leading to the fully hydrogenated products **e**.

The structures of all the intermediates involved in the reaction pathway and of the corresponding transition states have been optimized by DFT geometry, and activation energies for the various reaction steps have been calculated.

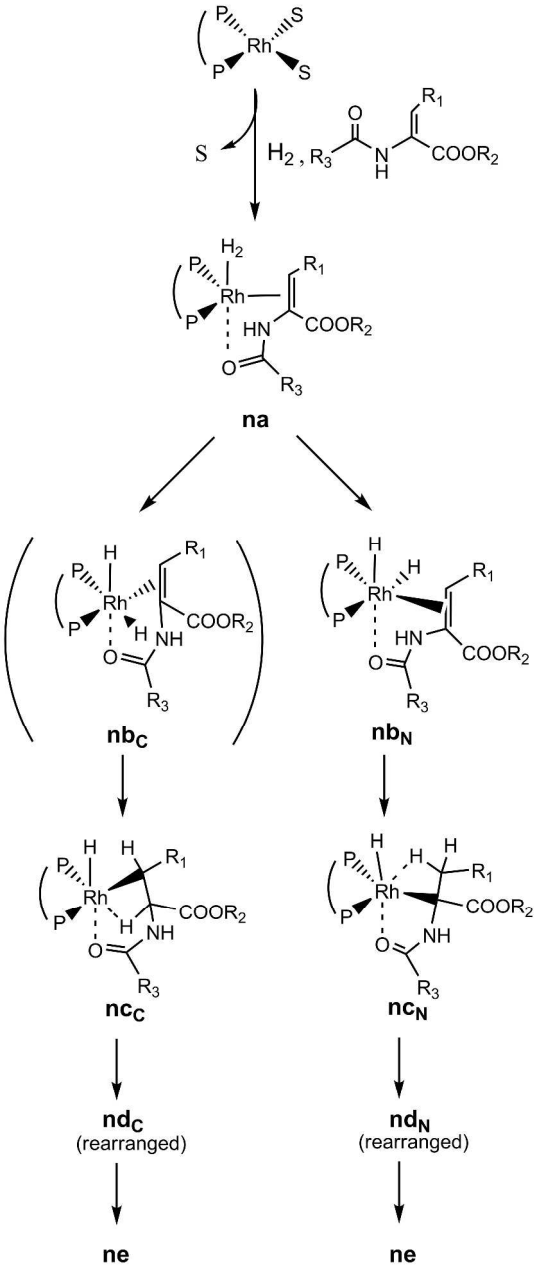

Scheme 1**. LNa** (N = 0-11) hydrogenation mechanism. S=solvent; (= diphenylphosphinobutane

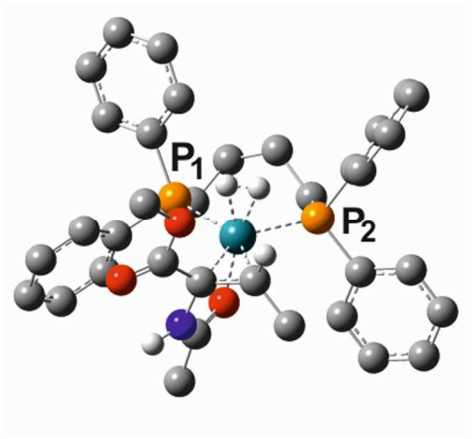

Figure 2. Optimized structure of the η^2-H_2 Rh complex **0a**; non-relevant hydrogen atoms are omitted for clarity.

The [1,4-bis(diphenylphosphino)butane](η^2-H_2)(**L0a)**Rh^+ complex (**0a**) has a pentacoordinated trigonal bipyramidal structure, similar to the one previously reported for (DuPHOS)(η^2-H_2)Rh^+,[23] and [1,4-bis(diphenylphosphinobutane)](η^2-H_2)Rh^+.[24,12] In **0a**, the remaining axial coordination site is not occupied by a solvent molecule but by the oxygen atom of the acetamido moiety (Figure 2), yielding a five-membered ring, including the Rh atom. The other oxygen atoms of **L0a** may potentially coordinate the metal in place of the acetamido one as well, but in this case more constrained four-membered rings would be formed, and this kind of coordination is thus not energetically favored. Due to the overall asymmetry of the complex, two very similar structures with a local minimum of energy have been computationally found. In the first one the ester group is placed in the equatorial plane that includes the Rh-alkene moiety on the same side of phosphorous P_1 (Figure 2), while in the second one it is on the opposite side. However, these two structures have almost the same energy (0.84 kJ/mol of difference) and therefore they can be considered equivalent.

Starting from the DFT optimized structure of the intermediate η-H_2 complex **0a**, the transition states (TS) leading to the intermediates **0b** (**0a**$_C^{TS}$ and **0a**$_N^{TS}$) have been computed.

For the "C route", the optimized TS structure **0a**$_C^{TS}$ is only 7.7 kJ/mol higher in energy than **0a** (Figure 3). **0a**$_C^{TS}$ has only one imaginary frequency at 600i cm^{-1}, and its vibrational mode is associated with the reaction coordinate that involves motion of the H_2 hydrogen atoms towards the cleavage of the H-H bond and the formation of two Rh-H bonds. All attempts to identify the **0b**$_C$ intermediate failed. Then it seems that in the "C route" the monohydrogenated complex **0c**$_C$ is formed directly from **0a**, in an apparent barrierless process, as previously reported.[24] Same results have been found for all the considered ligands. In the mono-hydrogenated product **0c**$_C$ the newly formed C-H bond lies in the Rh equatorial plane and gives rise to an agostic Rh···H-C in plane interaction (2.070 Å), allowing the Rh atom to maintain a pseudo-octahedral coordination structure (Figure 3). The intermediate product **0c**$_C$ is 87.7 kJ/mol more stable than **0a**. The energies of the **8c**$_C$, **9c**$_C$ and **11c**$_C$ intermediates have also been evaluated and are reported in Table 2.

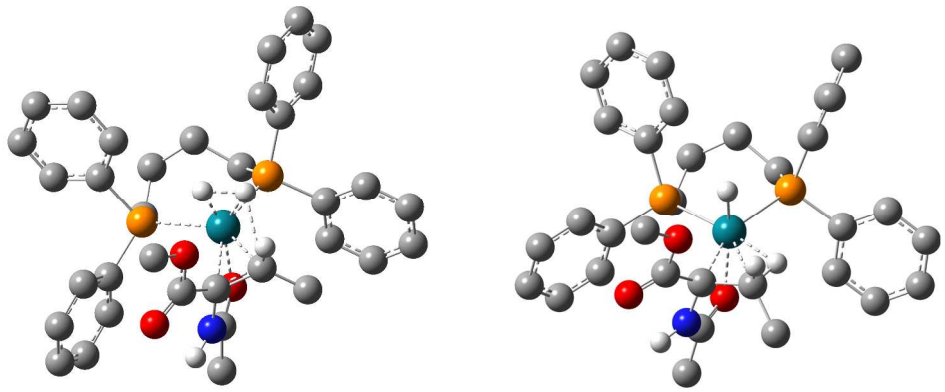

Figure 3. **0a**$_C^{TS}$ (left) obtained using **0a** as starting molecule and the optimized intermediate product **0c**$_C$ (right).

#	R_1	R_2	R_3	a^{TS}	b	b^{TS}	c	c^{TS}	d	d^{TS}	e
$\mathbf{9}_N$	CH_3	CH_3	H	10.6 (551i)	–18.8	15.1 (636i)	–46.5	14.0 (51i)	–67.8	41.7 (773i)	_ 121.9
$\mathbf{9}_C$				10.4 (624i)	-	0	–78.8	31.6 (41i)	–80.5	56.1 (799i)	
$\mathbf{0}_N$	CH_3	CH_3	CH_3	6.4 (550i)	–27.0	20.1 (584i)	–49.6	13.4 (39i)	–69.4	44.9 (778i)	_ 119.4
$\mathbf{0}_C$				7.7 (600i)	-	0	–87.7	38.0 (24i)	–85.8	56.9 (838i)	
$\mathbf{8}_N$	CH_3	CH_3	Ph	5.9 (595i)	–19.8	18.6 (584i)	–41.7	9.1 (38i)	–65.9	51.9 (763i)	_ 110.0
$\mathbf{8}_C$				6.9 (648i)	-	0	–89.0	41.2 (24i)	–82.6	59.2 (812i)	
$\mathbf{1}_N$	Ph	CH_3	Ph	10.4 (481i)	–25.8	22.6 (617i)	–34.1		–83.5	52.6 (837i)	–139.4
$\mathbf{2}_N$	Ph	CH_3	CH_3	11.9 (472i)	–23.7	21.0 (637i)	–43.0		–74.8	34.0 (854i)	–139.7
$\mathbf{3}_N$	Ph	CH_3	H	9.2 (454i)	–26.8	20.2 (619i)	–50.1	10.5 (28i)	–81.4	36.2 (823i)	–150.3
$\mathbf{4}_N$	Ph	CH_3	t-BuO	11.4 (471i)	–28.8	24.5 (652i)	–42.1	13.6 (20i)	–86.5	45.7 (847i)	–155.7
$\mathbf{11}_N$	H	CH_3	CF_3	3.3 (670i)	–27.9	14.2 (656i)	–70.9	12.9 (46i)	–81.2	37.1 (790i)	_ 156.2
$\mathbf{11}_C$				8.0 (576i)	-	0	–93.2	37.0 (31i)	–93.7	62.2 (832i)	

Table 2. Energies (in kJ/mol) of the dihydride (**b**), mono- (**c** and **d**) and dihydrogenated (**e**) intermediates relative to the starting dihydrogen compounds (**a**). For transition states barrier energies relative to the preceding structure (in kJ/mol) and imaginary frequencies (cm^{-1}) are reported.

For the "N route", the $\mathbf{0a_N}^{TS}$ transition state is characterized by an energy barrier of 6.4 kJ/mol, imaginary frequency at 550i cm^{-1}. Its vibrational mode leads to the dihydride $\mathbf{0b_N}$ (27.0 kJ/mol more stable than **0a**), that in turn gives the monohydrogenated species $\mathbf{0c_N}$ *via* the TS $\mathbf{0b_N}^{TS}$ with an activation energy of 20.1 kJ/mol and imaginary frequency of 584i cm^{-1} (Figure 4). The intermediate product $\mathbf{0c_N}$ is 49.6 kJ/mol more stable than **0a**, and shows an agostic Rh···H-C in plane interaction (2.363 Å). In both $\mathbf{0c_N}$ and $\mathbf{0c_C}$ the oxygen of the amidic carbonyl group still interacts with the metal center in axial position, now affording a five and a six-membered ring, respectively. Analogous results have been found for **L1**, **L2**, **L3**, **L4**, **L8**, **L9** and **L11**; the energies of the involved transition states and intermediates are reported in Table 2.

The final hydrogenation steps proceed firstly *via* the rotation around the Rh-C bond, giving **0d**, which in turn undergoes the final hydrogen transfer from the hydride moiety.

In the "C route", the substrate in $\mathbf{0c_C}$ rotates around the Rh-C bond bringing the oxygen of the amido group from the coordination site below the Rh plane to the equatorial plane (*via* $\mathbf{0c_C}^{TS}$, activation energy of 38.0 kJ/mol and imaginary frequency of 24i cm^{-1}). The resulting species $\mathbf{0d_C}$ is slightly less stable than $\mathbf{0c_C}$ (1.9 kJ/mol). However, the second hydrogen transfer from $\mathbf{0d_C}$ occurs *via* $\mathbf{0d_C}^{TS}$ with an activation energy of 56.9 kJ/mol (838i cm^{-1}), resulting in the final dihydrogenated product **0e** that is 119.4 kJ/mol more stable than the starting **0a**. An alternative pathway, leading directly from $\mathbf{0c_C}$ to **0e**, without the rotation of the ligand, is also possible, but in this case a very high energy barrier of 114.1 kJ/mol is found (the TS has a single imaginary frequency at 902i cm^{-1}, it is 26.4 kJ/mol less stable than **0a**, and its vibrational mode is associated with the reaction coordinate that involves motion of the hydride towards the formation of the second C-H bond). Similar results have been obtained for complexes **9a**, **8a** and **11a**.

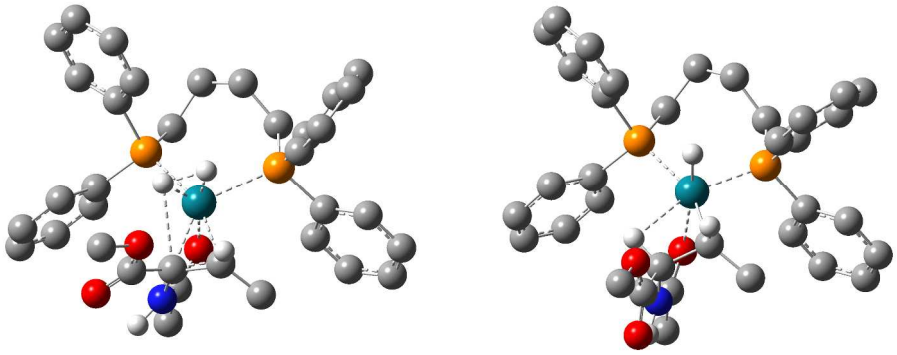

Figure 4. $\mathbf{0a_N}^{TS}$ (left) obtained using **0a** as starting molecule and the optimized intermediate product $\mathbf{0c_N}$ (right).

In the "N route", the transition state involved in the ligand rotation, $\mathbf{0c_N}^{TS}$, has an activation energy of 13.4 kJ/mol (imaginary frequency at 39i cm^{-1}), and affords the intermediate $\mathbf{0d_N}$, which is 19.8 kJ/mol more stable than $\mathbf{0c_N}$. Therefore, the energy required for the rearrangement of **0c** to give **0d** is much lower for the "N route" than for the "C route". $\mathbf{0d_N}$ then undergoes the second hydrogen transfer, *via* the $\mathbf{0d_N}^{TS}$ transition state, characterized by an activation energy of 44.9 kJ/mol (imaginary frequency of 778i cm^{-1}, see Figure 5). The calculated energies for other ligands (**L1**, **L2**, **L3**, **L4**, **L8**, **L9**, **L11**) are reported in Table 2.

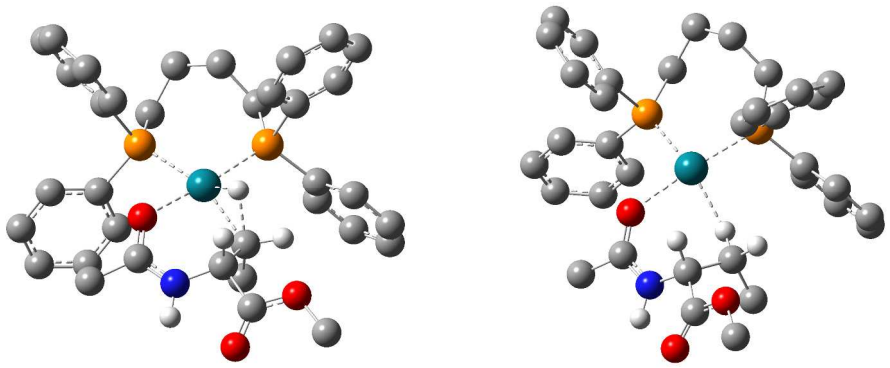

Figure 5. $\mathbf{0d_N}^{TS}$ and the fully hydrogenated product **0e**.

In **0e**, the fully hydrogenated substrate is still weakly coordinated to the Rh metal *via* the oxygen on its equatorial plane (2.199 Å) and the agostic H (2.103 Å) interactions, both in the "C route" and in the "N route", but only in the latter case the solvent (which has not been taken into account up to now) should easily replace the hydrogenated product **0e**.

The overall energy diagram of the hydrogenation reaction is reported in Figure 6.

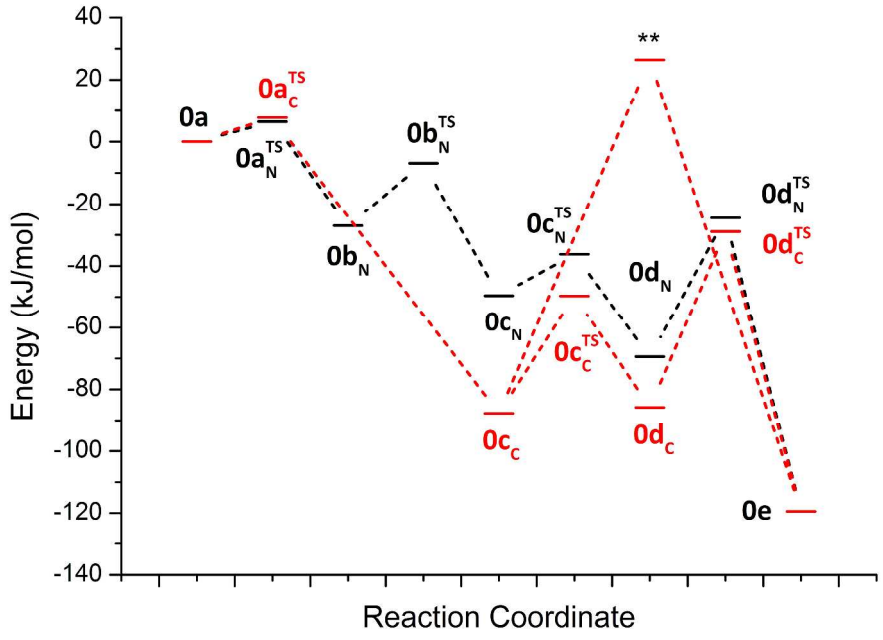

Figure 6. Schematic energy diagram for the complete hydrogenation reaction, as from computational results. Red: "C route"; black: "N route". **: the direct pathway from $\mathbf{0c_C}$ to **0e** (no rearrangement) is possible but energetically unfavored.

Discussion

The hydrogenation mechanism involves the formation of four reaction intermediates, from the η-H_2 complex (**a**) to the dihydride species (**b**) to the monohydrogenated derivative (**c**), which

successively undergoes the rearrangement process (**d**) before the second H transfer takes place. Two routes are possible depending on the ligand moiety the first H atom is transferred to.

As expected, the η-H_2 complexes have very short lifetimes, being quickly transformed into the corresponding dihydride derivatives. The "N route" appears slightly more favoured than the "C route", although the dihydride complexes $\mathbf{b_C}$ evolve to the monohydrogenated species $\mathbf{c_C}$ apparently without activation energy. In the case of the "N route" the involved activation energies are anyway very low, being between 14.2 and 24.5 kJ/mol. The monohydrogenated species $\mathbf{c_C}$ are more stable than the corresponding $\mathbf{c_N}$ ones. This is because the agostic Rh-H interaction is much stronger in $\mathbf{c_C}$ than in $\mathbf{c_N}$. For example, in $\mathbf{0c_C}$ and in $\mathbf{0c_N}$ the Rh-H distances are 2.070 and 2.363 Å, and the just formed C-H bonds are 1.135 and 1.092 Å, respectively. For complexes **9**, **0** and **8** the energy required for the rearrangement of **c** to give **d** is much lower for the "N route" (14.0, 13.4 and 9.1 kJ/mol, respectively) than for the "C route" (31.6, 38.0 and 41.2 kJ/mol). For this reason only the "N route" has been considered for calculations involving the other substrates.

Further indication that the "N route" is more favored with respect to the "C route" comes from the observation that, whereas in the $\mathbf{d_C}$ intermediates all the Rh coordination sites are occupied (with the unsaturated C and the O of the amido moiety on the equatorial plane and the O of the ester moiety below the plane), in $\mathbf{d_N}$, after the rotation, an axial coordination site below the equatorial plane is available for coordination of a solvent molecule. The quite pronounced solvent effect on the reaction rate observed when going from acetone/methanol/water to chloroform may therefore be taken as a further evidence of the predominancy of the "N-route". Other solvents characteristics (such as solvent viscosity or hydrogen solubility) may in principle affect the reaction rate. Nevertheless the employed solvents at the reaction temperatures used

here have very similar viscosities (ranging between 0.3 and 0.55 Pa*s, having acetone at RT and chloroform at 333K – the best and the worst solvent respectively for what concerns the reaction rate – viscosity values of 0.306 and 0.39 Pa*s respectively),[13] and the higher hydrogen pressure used for reactions in water should compensate for the lower solubility in this solvent with respect to the organic ones (the time for reaction completion is actually the same in water, acetone and methanol).

On this basis, the effect of R_3 on the ^{1}H PHIP patterns may be taken as a reporter of the extent of an asymmetrical relaxation process unbalancing the spin levels populations**,** occurring during the hydrogenation reaction.[25] Hydrogenation reactions catalyzed by complexes of the type (diphosphine)(diene)Rh^+ are known to proceed *via* the so-called "unsaturate route":[26] first, the unsaturated substrate coordinates the metal center of the catalyst, then molecular H_2 enters the coordination sphere and it is transferred to the substrate. The transfer is very fast, thus allowing to preserve some polarization up to the final hydrogenated product. The amount of lost polarization is related to the lifetime of intermediates. The redistribution of the spins among the energy levels which leads to adsorption/emission ^{1}H signals even in ALTADENA conditions (when only net signals are expected) can take place in intermediates in which the two parahydrogen atoms are magnetically non equivalent, if their lifetime is long enough.

As shown by the DFT calculations, some intermediates along the reaction pathway are stabilized by specific interactions of the metal with the ligand and/or with the solvent, thus increasing their lifetimes. Among these, **b**, **c** and **d** contain the two parahydrogen atoms in magnetically non equivalent positions. The effect of R_3 on the PHIP pattern may be accounted for by the interaction of the amido carbonyl group with the metal center, occurring in these three species, as found by Giernoth et al.,**[12]** leading to a stabilization of the intermediate which is

dependent on the electronic and/or steric properties of R_3. The stronger the CO-Rh interaction, the longer the intermediate lifetime and hence the efficiency of the asymmetrical relaxation process leading to the change in the spin populations and hence to antiphase ^1H signals in ALTADENA experiments.

The short lifetimes of the dihydride species **b** suggest that these intermediates play a limited role in determining the observed PHIP patterns. On the other hand, it is reasonable to think that in **c** and **d** the interaction of the amido carbonyl group in axial position with the metal center is effective in stabilizing these intermediates, as it yields a five/six membered ring. The molecular rearrangement in **c** to yield **d** and the transfer of the second H atom in **d** to yield **e** are the slowest reaction steps. Altogether, these considerations support the view that the intermediates **c** and/or **d** are those in which the redistribution of the spins among the nuclear levels due to asymmetrical relaxation can take place, to a different extent depending on the strength of the stabilization and/or on the effect of the axial interaction on the following reactions steps, either before (**c** species) or after (**d** species) the substrate rotation takes place.

As the PASADENA-like pattern is observed when R_3=Ph, but not when R_3=CH_3, H (see figure 1a, 1b and 1c), one may surmise that the lifetimes of **c** and/or **d** apparently become longer by increasing the steric hindrance of R_3. One may think that bulkier R_3 substituents induce slower rotation of the ligand during the transfer of the second hydrogen atom to the substrate, thus preventing the rapid evolution to **d**, and finally to **e**. As DFT calculations suggest that the slowest reaction step is the last one (from **d** to **e**), a further important contribution to the observed behaviour derives from the electronic properties of R_3, and in turn from its ability to stabilize intermediates **d** by the axial Rh-O interaction.

R_1 does not affect the PHIP pattern (net or antiphase signals), but it influences the overall reaction rate, causing a lowering in the signal enhancements of all the protons on going from R_1 = Ph (**L3**) to R_1 = Me (**L9**) to R_1 = H (**L10**). This trend is in accordance with the computed activation energies of the last hydrogenation step, which become progressively higher from **L3** to **L9** to **L10** (table 2). Being the T_1 values for the three hydrogenated products quite similar, the polarization loss is higher for compounds with the longer-living intermediates **d**.

L11 appears as a different case, as the electron-withdrawing properties of the CF_3 group in R_3 affect the overall reaction mechanism. The transition state $\mathbf{11a}^{TS}$ has a very low energy barrier (only 3.3 kJ/mol), with the last hydrogenation step being among the lowest energy barriers (37.1 kJ/mol). This allows the polarization to be preserved even in the presence of the strong dipolar interactions of the three proton resonances of the methyl group in the product.

There are other possible mechanisms leading to antiphase signals in ALTADENA experiments. Among these, the non-adiabacity of sample transfer from low to high magnetic field may play a role in the present case due to the use of manual transfer, which may be subjected to variations from one sample to the other. Nevertheless, the procedure has been accurately standardized and each sample measurement has been repeated many times in order to rule out any effect of manual errors.

On the other hand, we can not completely rule out a contribution from the possible continuation of reactions inside the magnet, during the few seconds interpassing between the insertion of the sample in the NMR magnet and the spectrum acquisition. This would lead to antiphase signals for those systems where the intermediates are longer-lived and hence the reaction rate is lower.

Conclusions

In summary, from the analysis of experimental PHIP data and theoretical calculations on a number of variously substituted dehydroamino acids, new insights into the hydrogenation pathway and the effect of the protective groups on the reaction rates and intermediates lifetimes have been gained. Even though the "C route" cannot completely be ruled out, there are strong indications that the operating mechanism follows the "N route", i.e. the first hydrogen transfer occurs to the α carbon atom of the alkene. A molecular rearrangement in the monohydrogenated intermediate **c** to give **d** occurs, and, together with the second H transfer to yield the final fully hydrogenated products, it is the slowest reaction step. A strong dependence of the PHIP pattern on the nature of the amino protecting group has been shown: there is a delicate relationship between the bulkiness of the substituent, its donating/withdrawing electronic properties and the lifetime of the monohydrogenated intermediates **c** and **d**, in which a redistribution of the spin populations among the energy levels can occur, thus yielding antiphase patterns of the PHIP signals in the ^{1}H NMR spectra of the products, even if the reactions are carried out under ALTADENA conditions. We can not completely rule out that this pattern is due to a lowering of the reaction rate induced by the different substituents, which would cause the reaction to partially proceed after introduction of the sample in the magnet.

The information gained in this work should be taken into account when designing unsaturated precursors of amino acids to be parahydrogenated with the aim of preparing hyperpolarized ^{13}C-amino acids, as the redistribution of the spin populations, occurring at some stage of the reaction

pathway, and the lowering of the overall reaction rate due to stabilization of intermediates has to be minimized in order to attain the highest ^{13}C polarization in the products.

The presence of a strong electron-attractor amino protecting group, promoting a faster reaction, yields positive consequences on the observed polarization. It is worth to note that the trifluoroacetic protection is easy to remove by hydrolysis, which is of importance for the preparation of unprotected hyperpolarized amino acids by parahydrogenation of unsaturated precursors followed by hydrolysis of the protective groups.

Experimental Section

^{1}H and ^{13}C NMR spectra were recorded on a JEOL EX-400 spectrometer operating at 400 MHz for ^{1}H and 100 MHz for ^{13}C respectively. For para-H_2 experiments, single scan ^{1}H spectra were acquired. Signal enhancements were calculated by comparing absolute integrals in the ^{1}H PHIP spectra and in reference spectra acquired after complete relaxation using the same NMR parameters. T_1 values were measured on degassed samples by the inversion recovery experiment at 14 T, 298K .

Solvents were stored over molecular sieves and purged with nitrogen before use. Hydrogen was produced by a CLAIND generator, model HG300.

Para-enriched hydrogen (about 51%) was prepared storing H_2 over Fe_2O_3 at 77 K for one hour.

Parahydrogenation reactions were carried out in ALTADENA[21] conditions in a 5 mm NMR tube equipped with a Young valve. For experiments in organic solvents, [1,4-bis(diphenylphosphino)butane](1,5-cyclooctadiene)rhodium(I) tetrafluoroborate (1 mg) was dissolved in acetone-d_6 or CD_3OD or $CDCl_3$/acetone-d_6 5:1 (0.4 mL), and activated by reaction

with H_2. The solution was then frozen and degassed, and the substrate (0.004 mmol) and the para-H_2 enriched mixture (4 atm) were added. For experiments in water, the substrates were added to 0.4 ml of a 2mM solution of [(1,4-bis[(phenyl-3-propanesulfonate)phosphine]butane](norbornadiene)rhodium(I) tetrafluoroborate in D_2O, prepared according to the published method,[8] under Ar atmosphere, and para-H_2 (8 atm) was added. The hydrogenation was carried out by shaking the tube for 10 seconds at RT in acetone-d_6 and CD_3OD, 333 K in $CDCl_3$/acetone-d_6 and 353 K in D_2O. All the experiments have been repeated three times under the same reaction conditions in order to check reproducibility. No relevant variation was observed.

Hydrogenation yields were evaluated by reacting the substrates with normal hydrogen under the same experimental conditions used for reactions with parahydrogen and measuring the amounts of product and (if present) remaining substrate at successive reaction times (5, 10, 15 seconds shaking, and 60 seconds for reactions in chloroform) by ^{1}H NMR. In all cases except for chloroform solutions, conversion was complete after 10 seconds shaking.

Calculations were performed with the Gaussian 09 (G09) program package[27] employing the DFT method with Becke's three parameter hybrid functional[28] and Lee-Yang-Parr's gradient corrected correlation functional[29] (B3LYP). The LanL2DZ basis set and effective core potential were used for the Rh atom, and the split-valence 6-31G** basis set was applied for all other atoms. Geometries of the complexes were optimized in the gas phase without any constrain, and the nature of all stationary points was confirmed by normal-mode analysis. Thermal correction based on harmonic frequencies and Gibbs free energy calculations were performed at 298.15 K and 1 atm. The nature of transition states were confirmed by harmonic vibrational frequency

calculations and normal-mode analyses, which gave for each of all transition states herein presented a single value of imaginary frequency.

Synthetic procedures

(Z)-methyl 2-benzamido-3-phenylacrylate (**L1**), (Z)-methyl 2-acetamido-3-phenylacrylate (**L2**), (Z)-methyl 2-formamido-3-phenylacrylate (**L3**), (Z)-2-benzamido-3-phenylacrylic acid (**L5**), (Z)-2-acetamido-3-phenylacrylic acid (**L6**), and methyl 2-formamidoacrylate (**L10**) were prepared according to literature procedures.[30,26]

(Z)-methyl 2-(tert-butoxycarbonylamino)-3-phenylacrylate (**L4**)[27]

0.55 g (2.51 mmol) of di-tert-butyl dicarbonate and a catalytic amount of 4-(dimethylamino)pyridine (0.03 g, 0.23 mmol) were added to a stirred solution of **L3** (0.5 g, 2.28 mmol) in 13 mL of acetonitrile, and the solution was stirred at room temperature for 3 hours. Acetonitrile was then evaporated and the residue was partitioned between water and diethyl ether. The aqueous phase was extracted with diethyl ether (2x30 mL). The combined organic layer was washed with brine (3x30 mL), dried over Na_2SO_4, filtered and the solvent was evaporated under reduced pressure. A pale yellow solid of (Z)-methyl 2-(N-(tert-butoxycarbonyl)acetamido)-3-phenylacrylate (0.67 g, 92%, ^{1}H NMR (acetone-d_6, 400 MHz): δ = 7.66 (1H, s, CH), 7.52 (2H, m, Ar), 7.43 (3H, m, Ar), 3.80 (3H, s, $COOCH_3$), 2.5 (3H, s, $COCH_3$), 1.29 (9H, s, 3xCH_3). ^{13}C NMR (acetone-d_6, 100 MHz): δ = 172.6 [C], 165.2 [C], 152.2 [C], 137.4[C], 134.0 [C,], 130.8 [CH], 130.0 [2xCH], 129.8 [2xCH], 128.3 [C], 83.8 [C] 52.7 [CH_3], 27.7 [3xCH_3], 26.1 [CH_3]) was obtained and used with no further purification.

0.46 mL (4.2 mmol) of N,N-dimethylethylene diamine were added to a stirred solution of 0.67 g (2.10 mmol) of (Z)-methyl 2-(N-(tert-butoxycarbonyl)acetamido)-3-phenylacrilate in 13 mL of acetonitrile, and the solution was stirred overnight at room temperature. Acetonitrile was then evaporated and the residue was partitioned between water and diethyl ether. The aqueous phase was extracted with diethyl ether (2x50 mL). The combined organic phase was washed with brine (3x50 mL), dried over Na_2SO_4, filtered and the solvent was evaporated under reduced pressure. The crude was then purified on silica gel using diethyl ether/petroleum ether 50/50 to afford **L4** as a white solid (0.47 g, 67%). ^{1}H NMR (acetone-d_6, 400 MHz): δ = 7.68 (2H, d, Ar), 7.41 (3H, m, Ar), 7.22 (1H, s, CH), 3.79 (3H, s, CH_3), 1.41 (9H, s, 3xCH_3). ^{13}C NMR (acetone-d_6, 100 MHz): δ = 166.8 [C], 154.4 [C], 135.1 [C], 132.0 [CH], 130.7 [2xCH], 129.9 [CH], 129.3 [2xCH], 127.3 [C], 80.2 [C], 52.5 [CH_3], 28.4 [3xCH_3]

(Z)-2-formamido-3-phenylacrylic acid (**L7**)

0.14 g of L3 were dissolved in 5 mL of methanol, and 15 mL of a 0.05 M NaOH in water were added. The mixture was stirred for 3 hours at room temperature. Methanol was then evaporated and the remaining water solution was acidified with HCl to pH=2. **L7** precipitated as a white solid and was collected by filtration. (0.100 g, 78%). ^{1}H NMR (acetone-d_6, 400 MHz): δ = 8.21 [1H, s, CHO], 8.74 (1H, bs, NH), 7.82 (2H, d, Ar), 7.38-7.32 (4H, m, 3xAr, CH). ^{13}C-NMR (acetone-d_6, 100 MHz): δ = 172.7 [C], 154.3 [C], 134.1 [C], 131.4 [CH], 129.6 [2xCH], 128.8 [CH], 130.2 [2xCH], 126.5 [C].

(Z)-methyl 2-benzamidobut-2-enoate (**L8**)

2-phenyloxazol-5(4H)-one (1g, 6.20 mmol, prepared according to the literature procedure)[28] was dissolved in 10 mL of dichloromethane and 0.68 mL (15.55 mmol) of acetaldehyde and 6.3 g (62 mmol) of Al_2O_3 were added. The mixture was stirred at room temperature for 24 h, then the alumina was filtered off and the solvent was evaporated under reduced pressure. The crude was purified on silica gel using diethyl ether/petroleum ether (40/60) to afford (Z)-4-ethylidene-2-phenyloxazol-5(4H)-one as a white solid (0.21 g, 20%). ^{1}H NMR (acetone-d_6, 400 MHz): δ = 8,07 (2H, d, Ar), 7.68 (1H, t, Ar), 7.59 (2H, t, Ar), 6.73 (1H, q, CH), 2.21 (3H, d, CH3).

0.2 mL of NaOMe 37% in methanol were added to a stirred suspension of (Z)-4-ethylidene-2-phenyloxazol-5(4H)-one (0.2 g, 1.1 mmol) in 3 mL of methanol. The solution was stirred at room temperature for 30 minutes and then methanol was evaporated. The residue was partitioned between a 10% aqueous solution of ammonium chloride and dichloromethane. The aqueous phase was extracted with dichloromethane (2x20 mL), the combined organic layers were washed with NH_4Cl (2x25 mL) and water (2x25 mL), dried over Na_2SO_4, filtered and the solvent was evaporated affording 0.2 g of **L8** as a dense colorless oil in 83% yield. ^{1}H NMR (acetone-d_6, 400 MHz): δ = 8.91 (1H, bs, NH), 8.00 (2H, d, Ar), 7.56 (1H, m, Ar), 7.48 (2H, m, Ar), 6.75 (1H, q, CH), 3.69 (3H, s, $COOCH_3$), 1.79 (3H, d, $CH\underline{CH_3}$). ^{13}C NMR (acetone-d_6, 100 MHz): δ = 166.2 [C], 165.5 [C], 135.0 [C], 134.1 [CH], 132.4 [CH], 129.2 [2xCH], 128.4 [2xCH], 127.0 [C], 52.2 [CH_3], 14.0 [CH_3].

(Z)-methyl 2-formamidobut-2-enoate (**L9**)[26]

0.50 g (2.95 mmol) of L-Threonine methyl ester hydrochloride and a catalytic amount of Et_3N (10 uL) were added to a stirred suspension of K_2CO_3 in methyl formate under argon atmosphere and the solution was stirred overnight at room temperature. The mixture was then filtered to

remove K_2CO_3 and methyl formate was evaporated under reduced pressure. The crude was purified on silica gel with 100% diethyl ether as eluent to afford 0.34 g of **L9** as a white solid (80%). ^{1}H NMR (acetone-d_6, 400 MHz): δ = 8.22 (1H, s, CHO), 6.69 (1H, q, CH), 3.71 (3H, $COOCH_3$), 1.74 (3H, d, $CH\underline{CH_3}$). ^{13}C NMR (acetone-d_6, 100 MHz): δ = 164.6 [C], 159.6 [C], 133.5 [CH], 127.2 [C], 52.6 [CH_3], 14.4 [CH_3]

Methyl 2-(2,2,2-trifluoroacetamido)acrylate (**L11**)

0.80 mL of Triethylamine (5.75 mmol) and 0.55 mL of ethyl trifluoroacetate (4.6 mmol) were added under Ar atmosphere to a stirred solution of methyl 2-amino-3-hydroxypropanoate hydrochloride (0.36 g, 2.3 mmol) in dry methanol. The reaction was quenched after 6 hours with aqueous HCl 0.1 M and diethyl ether was added. The aqueous phase was extracted with diethyl ether (2x40 mL) and the combined organic layers were washed with brine (2x40 mL), dried over Na_2SO_4, filtered and the solvent was evaporated under reduced pressure to afford a colorless oil (0.36 g, 72%) of methyl 3-hydroxy-2-(2,2,2-trifluoroacetamido) propanoate. ^{1}H-NMR (acetone-d_6, 400 MHz): δ = 8.53 (1H, bs, NH), 4.62 (1H, m, CH), 3.97 (2H, m, CH_2), 3.73 (3H, s, CH_3). ^{13}C-NMR (acetone-d_6, 100 MHz): δ = 170.1 [C], 157.8 [C, q, $^2J_{C\text{-}F}$ = 37.23 Hz], 116.9 [C, q, $J_{C\text{-}F}$ = 285.6 Hz], 61.8 [CH_2], 56.2 [CH], 52.8 [CH_3].

Methyl 3-hydroxy-2-(2,2,2-trifluoroacetamido)propanoate (0.35 g, 1.62 mmol) was dissolved in 10 mL of dry dichloromethane under Ar atmosphere. The solution was cooled at 0°C and 0.16 mL (2.02 mmol) of methanesulfonyl chloride and 0.68 mL (4.86 mmol) of triethylamine were slowly added; the mixture was then stirred for 3 hours at room temperature. The reaction was quenched with aqueous HCl 0.1 M. The aqueous phase was extracted with dichloromethane (2x40 mL) and the combined organic layers were washed with brine (2x40 mL), dried over

Na_2SO_4, filtered and the solvent was evaporated under reduced pressure to afford an orange liquid (0.100 g, 32%). ^{1}H-NMR (acetone-d_6, 400 MHz): δ = 9.33 (1H, bs, NH), 8.12 (1H, s, CHO), 6.11 (2H, s, CH_2), 3.85 (3H, s, CH_3). ^{13}C-NMR (acetone-d_6, 100 MHz): δ = 163.8 [C], 156.0 [C, $^2J_{C\text{-}F}$ = 40.7 Hz], 131.8 [C], 116.4 [C, q, $J_{C\text{-}F}$ = 287.5 Hz], 114.2 [CH_2], 53.5 [CH_3].

Acknowledgements

We gratefully acknowledge MIUR (PRIN2010, contract no. 2010B5B2NL) and Compagnia San Paolo (TO_call03_2012_0055) for financial support.

Supporting Information. ^{1}H PHIP spectra of **L5e**, **L6e**, **L7e**, **L10e** and **L11e** and T_1 values for **L3e**, **L5e**, **L6e**, **L7e**, **L9e**, **L10e** and **L11e** are available free of charge *via* the Internet at http://pubs.acs.org

AUTHOR INFORMATION

a: Department of Molecular Biotechnologies and Health Sciences, University of Torino, Via Nizza 52 – 10126 Torino – Italy

b: Department of Chemistry, University of Torino, Via Pietro Giuria 7 – 10125 Torino – Italy

Corresponding Authors

alessandra.viale@unito.it; carlo.nervi@unito.it

Author Contributions

The manuscript was written through contributions of all authors. All authors have given approval to the final version of the manuscript.

REFERENCES

(1) Abragam, A.; Goldman, M. Principles of Dynamic Nuclear Polarisation, *Reports on Progress in Physics* **1978**, *41*, 395-467.

(2) Ardenkjær-Larsen, J.-H.; Fridlund, B.; Gram, A.; Hansson, G.; Hansson, L.; Lerche, M.H.; Servin, R.; Thaning, M.; Golman, K. Increase in Signal-to-Noise Ratio of > 10,000 Times in Liquid-State NMR, *Proc. Natl. Acad. Sc.* **2003**, *100*, 10158-10163.

(3) Brindle, K.M.; Bohndiek, S.E.; Gallagher, F.A.; Kettunen, M.I. Tumor Imaging using Hyperpolarized ^{13}C Magnetic Resonance Spectroscopy, *Magn. Reson. Med.* **2011**, *66*, 505-519.

(4) Duckett, S.B.; Sleigh, C.J. Applications of the Parahydrogen Phenomenon: A Chemical Perspective, *Progr. Nucl. Magn. Reson. Spectrosc.* **1999**, *34*, 71-92.

(5) Green, R.A.; Adams, R.W.; Duckett, S.B.; Mewis, R.E.; Williamson, D.C.; Green, G.G.R. The Theory and Practice of Hyperpolarization in Magnetic Resonance using Parahydrogen, *Progr. Nucl. Magn. Reson. Spectrosc.* **2012**, *67*, 1-48.

(6) Viale, A.; Aime, S. Current Concepts on Hyperpolarized Molecules in MRI, *Curr. Opin. Chem. Biol.* **2010**, *14*, 90-96.

(7) Ellena, S.; Viale, A.; Gobetto, R.; Aime, S. Para-hydrogen Induced Polarization of Si-29 NMR Resonances as a Potentially Useful Tool for Analytical Applications, *Magn. Reson Chem.* **2012**, *50*, 529-533.

(8) Chen, A.P.; Kurhanewicz, J.; Bok, R.; Xua, D.; Joun, D.; Zhang, V.; Nelson, S.J.; Hurd, R.E.; Vigneron, D.B. Feasibility of Using Hyperpolarized [1-^{13}C]Lactate as a Substrate for in vivo Metabolic ^{13}C MRSI Studies, *Magn. Reson. Imag.* **2008**, *26*, 721-726.

(9) Chekmenev, E.Y.; Hoevener, J.; Norton, V.A.; Harris, K.; Batchelder, L.S.; Bhattacharya, P.; Ross, B.D.; Weitekamp, D.P. PASADENA Hyperpolarization of Succinic Acid for MRI and NMR Spectroscopy, *J. Am. Chem. Soc.* **2008**, *130*, 4212-4213.

(10) Gallagher, F.A.; Kettunen, M.I.; Day, S.E.; Lerche, M.; Brindle, K.M. ^{13}C MR Spectroscopy Measurements of Glutaminase Activity in Human Hepatocellular Carcinoma Cells using Hyperpolarized ^{13}C-Labeled Glutamine, *Magn. Reson. Med.* **2008**, *60*, 253-257.

(11) Jensen, P.R.; Karlsson, M.; Meier, S.; Duus, J.O.; Lerche, M.H. Hyperpolarized Amino Acids for In Vivo Assays of Transaminase Activity, *Chem. Eur. J.* **2009**, *15*, 10010-10012.

(12) Giernoth, R.; Einrich, H.; Adams, N.J.; Deeth, R.J.; Bargong J., Brown, J.M., PHIP Detection of a Transient Rhodium Dihydride Intermediate in the Homogeneous Hydrogenation of Dehydroamino Acids, *J. Am. Chem. Soc.* **2000**, *49*, 12381-12382.

(13) Dortmund Data bank, Oldenburg, http://www.ddbst.com/en/EED/PCP/VIS_C174.php, 21/10/2015

(14) Tang, J.A.; Gruppi, F.; Fleysher, R.; Sodickson, D.K.; Canary, J.W.; Jerschow, A. Extended Para-Hydrogenation Monitored by NMR Spectroscopy, *Chem. Commun.* **2011**, *47*, 958-960.

(15) Gruppi, F.; Xu, X.; Zhang, B.; Tang, J.A.; Jerschow, A.; Canary, J.W. Peptide Hydrogenation and Labeling with Parahydrogen, *Angew. Chem. Int. Ed.* **2012**, *51*, 11787-11790.

(16) Soon, P.C.; Xu, X.; Zhang, B.; Gruppi, F.; Canary, J.W.; Jerschow, A. Hyperpolarization of Amino Acid Precursors to Neurotransmitters with Parahydrogen Induced Polarization, *Chem. Commun.* **2013**, *49*, 5304-5306.

(17) Trantzschel, T.; Plaumann, M.; Bernarding, J.; Lego, D.; Ratajczyk, T.; Dillenberger, S.; Buntkowsky, G.; Bargon, J.; Bommerich, U. Application of Parahydrogen-Induced Polarization to Unprotected Dehydroamino Carboxylic Acids, *Appl. Magn. Reson.* **2013**, *44*, 267-278.

(18) Sauer, G.; Nasu, D.; Tietze, D.; Gutmann, T.; Englert, S.; Avrutina, O.; Kolmar, H.; Buntkowsky G. Effective PHIP Labeling of Bioactive Peptides Boosts the Intensity of the NMR Signal, *Angew. Chem. Int. Ed.* **2014**, *53*, 12941–12945.

(19) Gloggler, S.; Wagner, S.; Bouchard, L.-S. Hyperpolarization of Amino Acid Derivatives in Water for Biological Applications, *Chem. Sci.* **2015**, *6*, 4261-4266.

(20) Gloggler, S.; Muller, R.; Colell, J.; Emondts, M.; Dabrowski, M.; Blumicha B.; Appelt, S. Para-Hydrogen Induced Polarization of Amino Acids, Peptides and Deuterium–Hydrogen Gas, *Phys. Chem. Chem. Phys.,* **2011**, *13*, 13759–13764.

(21) Pravica, M.G.; Weitekamp, D.P. Net NMR Alignment by Adiabatic Transport of Parahydrogen Addition Products to High Magnetic Field, *Chem. Phys. Lett.* **1988**, *145*, 255-258.

(22) Bowers, C.R.; Weitekamp, D.P. Parahydrogen and Synthesis Allow Dramatically Enhanced Nuclear Alignment, *J .Am. Chem. Soc.* **1987**, *109*, 5541-5542.

(23) Feldgus, S.; Landis, C.R. Large-Scale Computational Modeling of $[Rh(DuPHOS)]^+$-Catalyzed Hydrogenation of Prochiral Enamides: Reaction Pathways and the Origin of Enantioselection, *J. Am. Chem. Soc.* **2000**, *122*, 12714-12727.

(24) Reineri, F.; Aime, S.; Gobetto, R.; Nervi, C. Role of the Reaction Intermediates in Determining PHIP (Parahydrogen Induced Polarization) Effect in the Hydrogenation of Acetylene Dicarboxylic Acid with the Complex $[Rh (dppb)]^+$ (dppb: 1,4-bis(diphenylphosphino)butane), *J. Chem. Phys.* **2014**, *140*, 094307

(25) Kating, P.; Wandelt, A.; Selke, R.; Bargon, J. Nuclear Singlet/Triplet Mixing during Hydrogenations with Parahydrogen: an in situ NMR Method to Investigate Catalytic Reaction Mechanisms and their Kinetics. 2. Homogeneous Hydrogenation of 1,4-dihydro-1,4-epoxynaphthalene using Different Rhodium Catalysts, *J. Phys. Chem.* **1993**, *97*, 13313-13317.

(26) Halpern, J.; Riley, D.P.; Chan, A.S.C.; Pluth, J.J. Novel Coordination Chemistry and Catalytic Properties of Cationic 1,2-bis(diphenylphosphino)ethanerhodium(I) Complexes, *J. Am. Chem. Soc.* **1977**, *99*, 8055-8057.

(27) Frisch, M.J. *et al*., *Gaussian 09. [Revision C.01],* **2009**. Wallingford CT, Gaussian, Inc.

(28) Becke, A.D. Density-Functional Thermochemistry. III. The Role of Exact Exchange, *J. Chem. Phys.* **1993**, *98*, 5648-5652.

(29) Lee, C.; Yang, W.; Parr, R.G. Development of the Colle-Salvetti Correlation-Energy Formula into a Functional of the Electron Density, *Phys. Rev. B: Condens. Matter* **1988**, *37*, 785-789.

(30) Jursic, B.S.; Sagiraju, S.; Ancalade, D.K.; Clark, T.; Stevens, E.D. Practical Preparation of Z-α-(N-Acetylamino)- and Z-α-(N-Benzoylamino)-α,β-unsaturated Acids, *Synth.Commun.* **2007**, *37*, 1709-1714.

(26) Panella, L.; Aleixandre, A.M.; Kruidhof, G.J.; Robertus, J.; Feringa, B.L.; de Vries, J.G.; Minnaard, A.J. Enantioselective Rh-Catalyzed Hydrogenation of N-Formyl Dehydroamino Esters with Monodentate Phosphoramidite Ligands, *J. Org. Chem*., **2006**, *71*, 2026-2036.

(27) Grehn, L.; Gunnarsson, K.; Ragnarsson, U. Removal of Formyl, Acetyl, and Benzoyl Groups from Amides with Conversion into the Corresponding t-butyl Carbamates, *J. Chem. Soc. Chem. Commun.* **1985**, 1317-1318.

(28) Conway, P.A.; Devine, K.; Paradisi, F. A Simple and Efficient Method for the Synthesis of Erlenmeyer Azlactones, *Tetrahedron* **2009**, *65*, 2935-2938.

Table of Contents

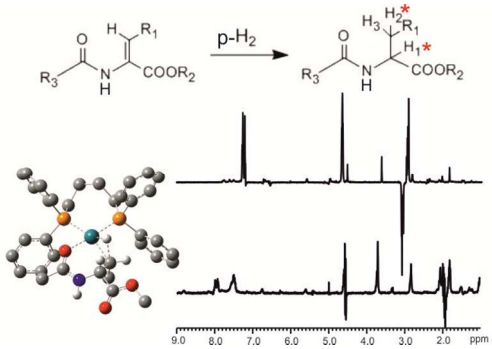

Parahydrogenation of a series of protected dehydroamino acids yields ^{1}H PHIP patterns which are strongly dependent on the steric and electronic properties of the amino protecting group, which affects the stability of intermediates.

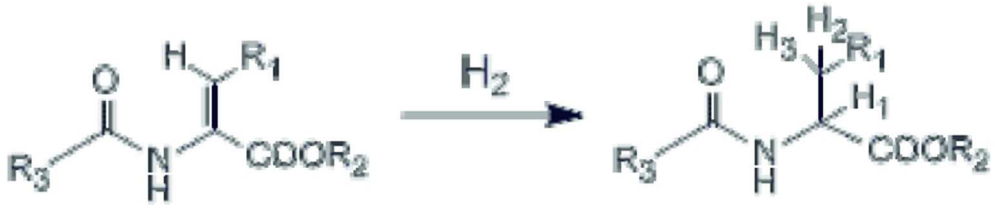

L1a: R_1 = Ph, R_2 = CH_3, R_3 = Ph — **L1e**
L2a: R_1 = Ph, R_2 = CH_3, R_3 = CH_3 — **L2e**
L3a: R_1 = Ph, R_2 = CH_3, R_3 = H — **L3e**
L4a: R_1 = Ph, R_2 = CH_3, R_3 = t-BuO — **L4e**
L5a: R_1 = Ph, R_2 = H, R_3 = Ph — **L5e**
L6a: R_1 = Ph, R_2 = H, R_3 = CH_3 — **L6e**
L7a: R_1 = Ph, R_2 = H, R_3 = H — **L7e**
L8a: R_1 = CH_3, R_2 = CH_3, R_3 = Ph — **L8e**
L9a: R_1 = CH_3, R_2 = CH_3, R_3 = H — **L9e**
L10a: R_1 = H, R_2 = CH_3, R_3 = H — **L10e**
L11a: R_1 = H, R_2 = CH_3, R_3 = CF_3 — **L11e**

Chart 1. Dehydroaminoacids for para-hydrogenation.
70x51mm (300 x 300 DPI)

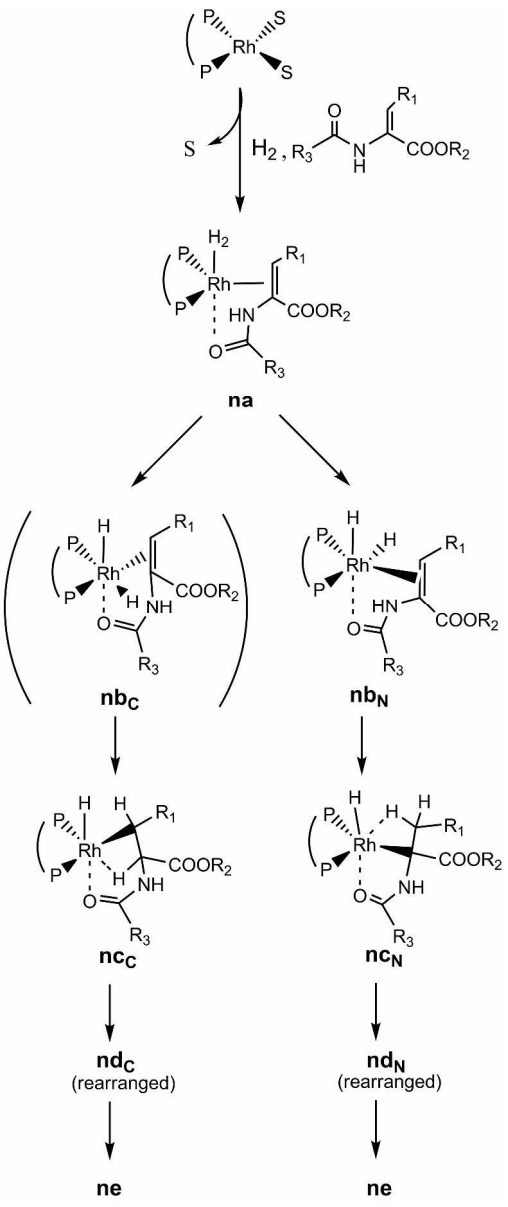

Scheme 1. LNa (N = 1-11) hydrogenation mechanism. S=solvent; (= diphenylphosphinobutane
205x488mm (600 x 600 DPI)

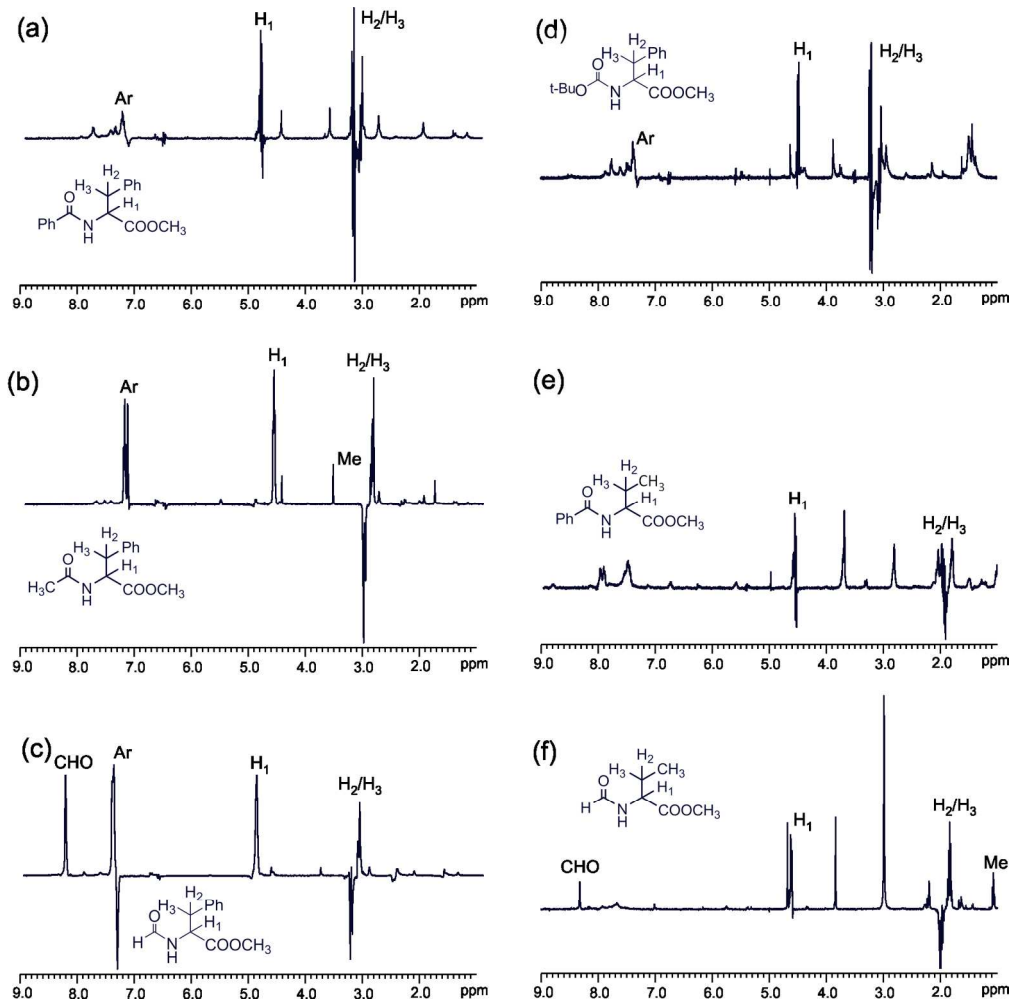

Figure 1: Single scan 1H NMR spectra of hyperpolarized (a) L1e, (b) L2e, (c) L3e, (d) L4e, (e) L8e and (f) L9e (10 mM solutions, RT, 9.4 T; acetone-d6). No additional information is present in the omitted parts of the spectra.
163x162mm (300 x 300 DPI)

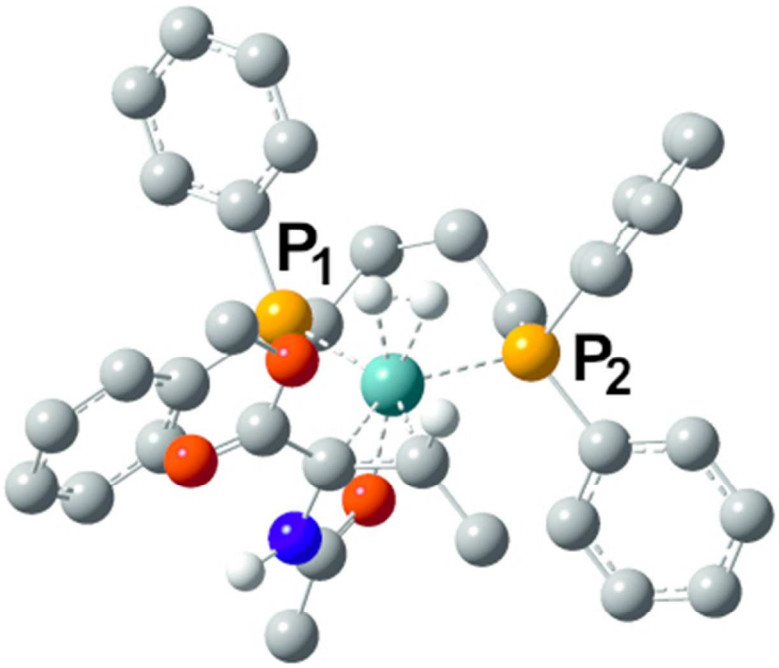

Figure 2. Optimized structure of the η2-H2 Rh complex 0a; non-relevant hydrogen atoms are omitted for clarity
34x32mm (300 x 300 DPI)

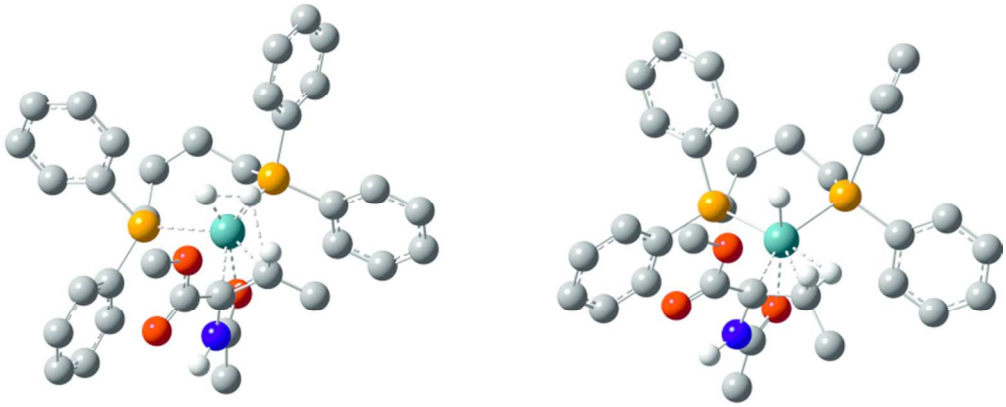

Figure 3. 0aCTS (left) obtained using 0a as starting molecule and the optimized intermediate product 0cC (right).
71x30mm (300 x 300 DPI)

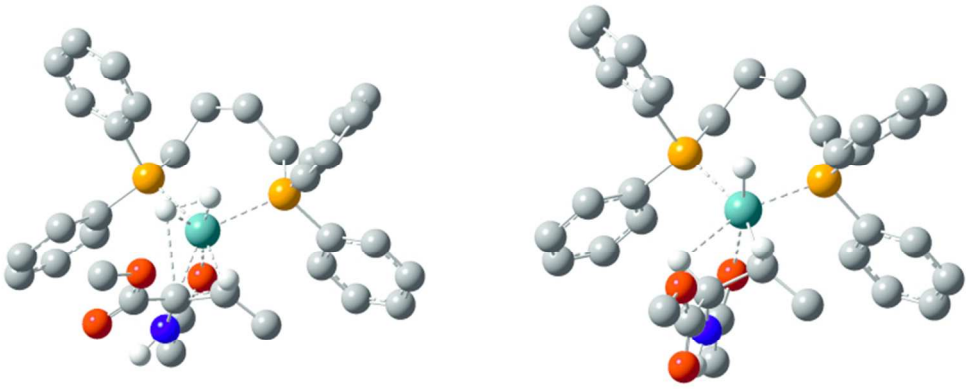

Figure 4. 0aNTS (left) obtained using 0a as starting molecule and the optimized intermediate product 0cN (right).

69x30mm (300 x 300 DPI)

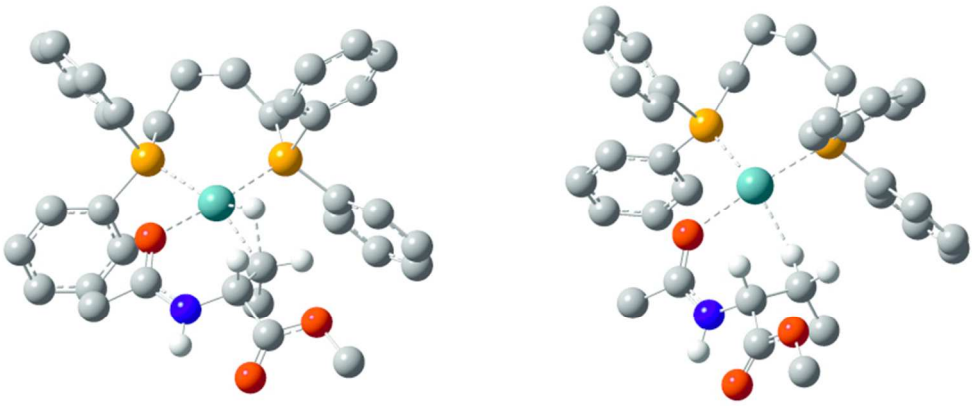

Figure 5. 0dNTS and the fully hydrogenated product 0e.
71x30mm (300 x 300 DPI)

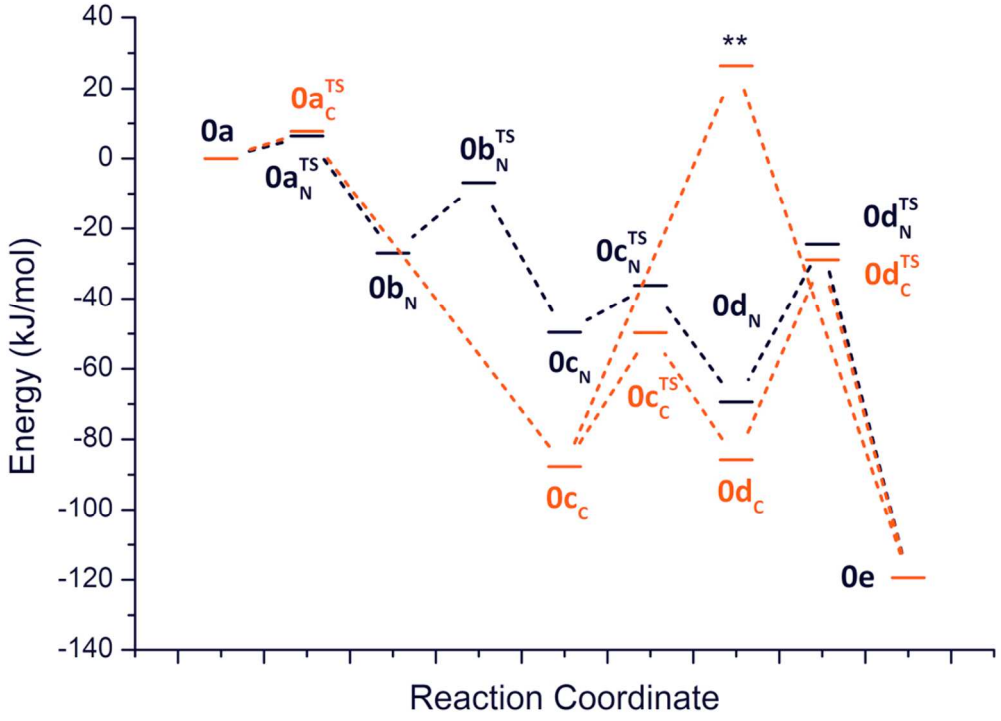

Figure 6. Schematic energy diagram for the complete hydrogenation reaction, as from computational results. Red: "C route"; black: "N route". **: the direct pathway from 0cC to 0e (no rearrangement) is possible but energetically unfavored.
92x67mm (300 x 300 DPI)

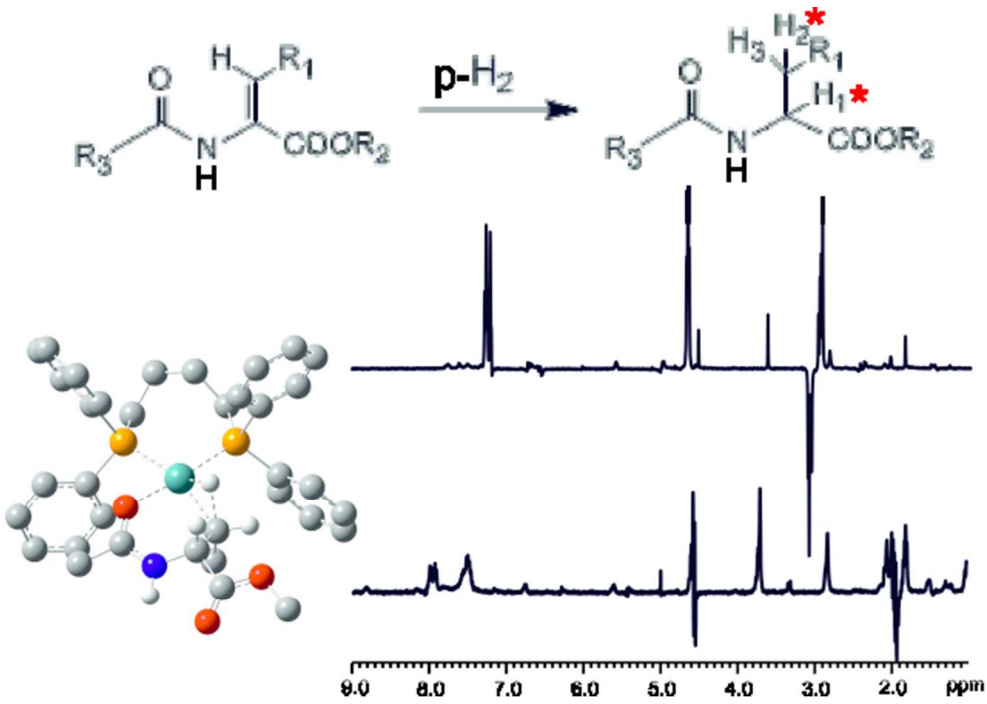

TOC
55x37mm (300 x 300 DPI)